Earthline Journal of Chemical Sciences
E-ISSN: 2581-9003; CODEN: EJCSB4
Volume 13, Number 3, August 2026, Pages 293-312
https://doi.org/10.34198/ejcs.13326.21.293312

Design of a bioactive nickel(II) complex based on a hydrazone Schiff base ligand: Synthesis, structural characterization and antimicrobial investigations

Abdoul Sall

Département de Chimie, Université Alioune Diop de Bambey, Sénégal

Moussa Faye

Département de Chimie, Université Alioune Diop de Bambey, Sénégal

Alassane Saïdou Diallo

Département de Chimie, Université Alioune Diop de Bambey, Sénégal

Ousmane Sall

Département de Chimie, Université Cheikh Anta Diop de Dakar, Sénégal

Farba Bouyagui Tamboura

Département de Chimie, Université Alioune Diop de Bambey, Sénégal

Moussa Dieng*

Département de Chimie, Université Alioune Diop de Bambey, Sénégal
e-mail: moussa.dieng@uadb.edu.sn

Mohamed Gaye

Département de Chimie, Université Cheikh Anta Diop de Dakar, Sénégal

Abstract

A novel hydrazone Schiff base ligand (H_3L) and its nickel(II) complex were synthesized and fully characterized using a range of spectroscopic techniques. The antibacterial activities of both compounds were evaluated against Gram-positive and Gram-negative bacterial strains by means of the agar diffusion method, minimum inhibitory concentration (MIC) assays, and minimum bactericidal concentration (MBC) assays. The nickel complex exhibited significantly enhanced antibacterial activity compared to the free ligand, an improvement that may be attributed to the chelation effect and the increased lipophilicity of the complex.

The present work aimed to synthesize a novel hydrazone Schiff base ligand and its nickel(II) complex, characterize their structures, and evaluate their antibacterial activities against selected pathogenic bacterial strains. The ligand (H_3L) crystallizes in the monoclinic system in the space group C2/c, with unit cell parameters a = 21.0113(2) Å, b = 6.9353(4) Å, c = 21.3996(9) Å, α = 90°, β = 104.202(2)°, γ = 90°.

Received: May 19, 2026; Accepted: June 22, 2026; Published online: July 7, 2026

Keywords and phrases: Nickel(II), antimicrobial, hydrazone.

*Corresponding author

1. Introduction

Acylhydrazone ligands occupy an important place in coordination chemistry owing to their ability to readily bind metal ions, forming stable and structurally diverse complexes. They are widely employed in bioinorganic chemistry and medicinal chemistry for the development of compounds with biological activities, including antibacterial and antiviral properties [1]. In catalysis, their metal complexes serve as effective systems for accelerating various chemical reactions, such as oxidations and organic cross-coupling reactions [2]. They also play an essential role in materials science, particularly in the construction of coordination networks and functional materials with optical, magnetic, or luminescent properties [3]. Notably, tridentate ligands bearing a hydroxyl group can generate extended structures in which the oxygen atom acts as a bridging ligand.

2. Chemical Context

Transition metal complexes of Schiff bases are attracting increasing interest due to their remarkable and diverse properties. Among these, pharmacological applications against Gram-positive bacteria in vitro have been extensively reported [4].

Schiff bases are widely used in coordination chemistry to prepare materials with tailored properties. Over the past decade, numerous compounds applicable in catalysis, magnetism, luminescence, and biological activity studies have been synthesized and thoroughly characterized [5].

The development of novel molecules with pharmacological activity and an acceptable safety profile remains a major challenge in the chemical and pharmaceutical sciences. Compounds bearing the hydrazone unit –C=N–NH–R are well known for their therapeutic versatility [6–9]. Metal coordination compounds derived from hydrazone ligands are also of great interest due to their broad pharmacological profile, encompassing antitumor [10], antimicrobial [11,12], and anti-tuberculosis [13] activities. It has been established that hydrazone ligands with intrinsic biological activity can exhibit significantly enhanced efficacy upon complexation with metal ions. Such ligands are widely used for the synthesis of complexes with valuable biochemical and physical properties [14-17].

Metal complexes incorporating o-vanillin derivatives display a wide range of biological activities [18] and are of interest in fields such as magnetism, catalysis, medicine [19], and luminescence. The presence of phenolic moieties suggests that these complexes may exhibit antioxidant properties, as reported in the literature [20], as well as antibacterial activity. The physical and chemical properties of metal complexes are governed both by their geometry and by the nature of the electron density around the metal center. In recent work, we have focused on the synthesis of ligands and their metal complexes for biological applications including antioxidant, antibacterial, and antimicrobial activity studies [21].

3. Experimental Section

3.1. Synthesis of H_3L

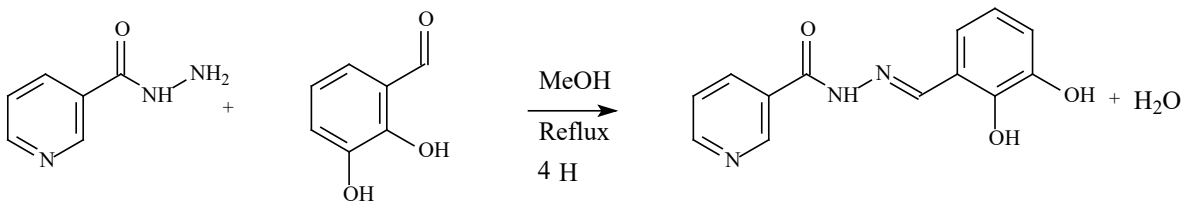

The H_3L ligand was synthesized from an equimolar mixture (6 mmol) of 2,3-dihydroxybenzaldehyde and nicotinohydrazide dissolved in 20 mL of methanol in the presence of a few drops of glacial acetic acid. The mixture was heated under reflux for 4 hours. A clear yellow solution was obtained, which precipitated upon the addition of 30 mL of diethyl ether. The precipitate was collected by filtration and dried over a P_2O_5 desiccant.

Appearance: white solid. M.p. = 178-180 °C

Mass: 1.121 g; yield: 76.71%

Molar mass: 257 g/mol

Empirical formula: $C_{13}H_{12}N_3O_3$

Solubility: The product is soluble in DMSO, DMF, ethanol, methanol, and acetonitrile.

Elemental analysis calculated: C = 60.70%; H = 4.31%; N = 16.33%.

Elemental analysis found: C = 60.72%; H = 4.16%; N = 15.97%.

^{1}H NMR (DMSO-d_6, δ in ppm): 7.43-8.63 (m, 7H, Ar-H and Py-H); 9.09 (s, 1H, C_1-OH); 8.78 (s, 1H, N–H); 14.37 (s, 1H, C_2-OH).

^{13}C NMR (DMSO-d_6, δ in ppm): 161.894 (C=O); 146.674 (C-OH); 146.127 (C-OH); 152.94 (C=N); 117–149 (CAr, Py).

3.2. Synthesis of the Ni(II) Complex

In a flask containing 5 mL of ethanol, 1 mmol of the metal salt $MX_2{\cdot}nH_2O$ (X = Cl, NO_3, OAc; n = 2 or 6; M = Cu, Mn, or Ni) was dissolved at room temperature. A solution of 1 mmol of the ligand (H_3L) was then added, and the mixture was stirred at room temperature for 2 hours. The resulting solids were collected by filtration, washed twice with diethyl ether (2 × 10 mL), and dried over P_4O_{10}. The filtrates from solutions were subjected to slow evaporation. The melting temperatures, yields, appearances, and colors of the complexes are listed in Table 1.

Table 1. Melting temperature, appearance, color, and yield of the ligand complexes.

Metal Salt	M.p. (°C)	Yield (%)	Appearance and Color
$CuCl_2{\cdot}2H_2O$	236	66	Black powder
$Ni(NO_3)_2{\cdot}6H_2O$	219	77	Green powder
$Mn(OAc)_2{\cdot}6H_2O$	250	55	Yellow powder

4. Results and Discussion

The topological structure of the H_3L ligand is shown in Scheme 1.

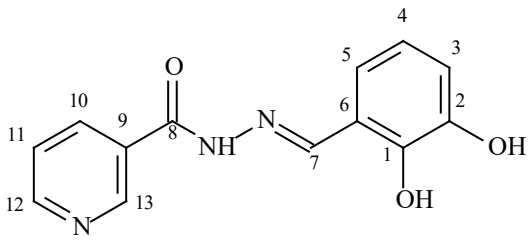

Scheme 1. Structure of the H_3L ligand.

4.1. Infrared Spectroscopy of the H_3L Ligand and the H_3L-Ni Complex

The IR spectrum of the ligand displays a broad band centered at 3329 cm^{-1}, attributed to the ν(O-H) stretching vibration of both the primary alcohol and phenolic functions [22]. A band at 3206 cm^{-1} is assignable to the ν(N-H) stretching vibration [23-25]. The intense band at 1632 cm^{-1} is assigned to the ν(C=N) stretching vibration of the imine function [26], confirming the occurrence of the condensation reaction that leads to ligand formation. The band at 1277 cm^{-1} is attributed to the phenolic ν(C–O) stretching vibration [27]. The carbonyl ν(C=O) band appears at 1663 cm^{-1}. The band at 1152 cm^{-1} is attributed to the ν(N-N) stretching vibration. Bands in the range 1609-1425 cm^{-1} and at 1520 cm^{-1} are assigned to ν(C=C) stretching vibrations of the aromatic ring [28]. A broad band at approximately 3600 cm^{-1} is attributable to the ν(O-H) stretching vibration of a free water molecule. Aromatic C-H out-of-plane deformation vibrations are observed at low frequencies, between 755 and 709 cm^{-1}. For the nickel(II) complex, the characteristic band of the ν(C=N) vibration goes from 1636 to 1614 cm^{-1} and that of ν(C-O) goes from 1277 to 1234 cm^{-1}.

4.2. ^1H NMR Spectrum of the H_3L Ligand

The ^1H NMR spectrum was recorded in DMSO-d_6. A signal at 7.59 ppm is attributed to the imine proton, supporting the formation of the Schiff base through the condensation reaction. Two singlets, each integrating for one proton, appear at 9.091 and 8.6 ppm, corresponding respectively to the two phenolic OH protons. The four aromatic ring protons resonate in the region δ, 6.7-8.2 ppm, and the NH proton appears at 8.78 ppm.

4.3. ^{13}C NMR Spectrum of the H_3L Ligand

The ^{13}C NMR spectrum was recorded in DMSO-d_6. It exhibits thirteen signals, consistent with the thirteen carbon atoms of the molecule. The signals at 146.674 and 161.894 ppm are attributed to the imine carbon C_7 and the carbonyl carbon C_9, respectively. The remaining signals, observed in the region 117-149 ppm, are assigned to the eleven carbon atoms of the pyridine and benzene rings. The phenolic carbon signal overlaps with that at 146.674 ppm.

4.4. Conductometric and UV-Visible Study of the H_3L Ligand and the H_3L-Ni Complex

The UV-Visible spectrum of the H_3L-Ni complex exhibits three principal absorption bands centered at approximately 318, 358, and 419 nm [29]. Compared with the free ligand, these bands clearly indicate the formation of the metal complex and the modification of the ligand electronic environment upon coordination.

- The intense absorption band observed at 318 nm is assigned to intraligand $\pi \rightarrow \pi^*$ transitions, mainly associated with the aromatic rings and the conjugated hydrazone system. Although this transition is also present in the free ligand, a slight bathochromic shift is observed after complexation, which can be attributed to enhanced electronic conjugation resulting from metal coordination [30].
- The second absorption band, located at 358 nm, is attributed to $n \rightarrow \pi^*$ transitions involving the nonbonding electron pairs of the donor atoms (N and O) of the ligand [31]. Relative to the free ligand, this band generally shifts toward longer wavelengths upon coordination, reflecting a decrease in transition energy caused by the interaction of the nitrogen and oxygen donor atoms with the metal center.
- The broad and low-energy band appearing at 419 nm is characteristic of the complex and is assigned to ligand-to-metal charge transfer (LMCT). The emergence of this new band, absent in the spectrum of the free ligand, provides strong evidence for complex formation [29].

Overall, the spectral changes observed between the free ligand and the nickel complex confirm the participation of the ligand donor sites in coordination. Metal binding promotes greater electronic delocalization and reduces the HOMO-LUMO energy gap, thereby explaining the bathochromic shifts observed in the absorption bands.

The Ni(II) complex displays a pronounced absorption band at 419 nm [29], characteristic of ligand-to-metal charge transfer. The spectroscopic data further suggest an octahedral geometry around the Ni(II) center, in agreement with the measured magnetic moment of approximately 3 μB, indicative of two unpaired electrons.

Conductivity measurements performed in DMF revealed a conductivity value of 8.3 $\Omega^{-1}.cm^2.mol^{-1}$ while maintaining neutral electrolyte characteristics [32]. This result demonstrates the stability of the complex in solution, indicating weak conductive behavior. This low conductivity suggests that the ligand behaves essentially as a non-electrolytic species in solution, exhibiting negligible ionic dissociation in DMF [33].

5. X-Ray Crystallographic Study of H_3L

Crystals suitable for X-ray diffraction were grown by slow evaporation of a methanol solution of the ligand. Details of the crystal structure solution and refinement are given in Table 2. A suitable single crystal was selected and mounted on a Bruker APEX-II CCD diffractometer using graphite-monochromated Mo Kα radiation (λ = 0.71073 Å). All data were corrected for Lorentz and polarization effects; no absorption correction was applied. Hydrogen atoms on water molecules and NH groups were located from difference Fourier maps and refined isotropically. Remaining hydrogen atoms were geometrically optimized and refined using a riding model with AFIX instructions.

Table 2. Crystal data and structure refinement parameters for the complex.

Parameter	**Value**
Formula	$Cl{\cdot}C_{13}H_{12}N_3O_3$, $2(H_2O)$
Crystal system	Monoclinic
Space group	C2/c
a (Å)	21.0113(2)
b (Å)	6.9353(4)
c (Å)	21.3996(9)
α (°)	90
β (°)	104.202(2)
γ (°)	90
Cell volume ($Å^3$)	3023.06
Z	8
R-factor (%)	5.52
Reflections collected	2946
μ(mm^{-1})	0.28

Independent reflections	2878 [R_{int} = 0.050. R_{sigma} = 0.0314]
$\theta_{max}/\theta_{min}$ (°)	26.4/2.0
GOF	1.0550
Final *R* Indices [$I > 2\sigma(I)$]	R_1 = 0.0552. wR_2 = 0.1339

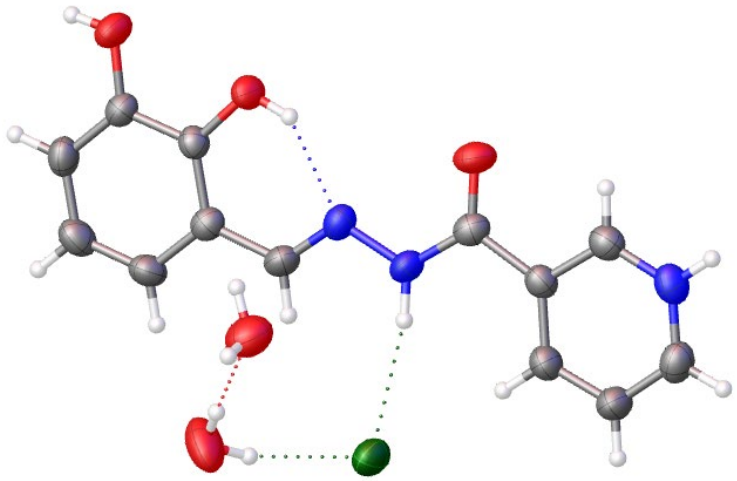

6. Antimicrobial Activity

The agar diffusion method is one of the oldest and most widely used approaches for determining the susceptibility of bacteria to antibiotics or synthetic compounds. It is applicable to the majority of pathogenic bacteria, including slow-growing strains, offers flexibility in the choice of antimicrobial agents, and requires no specialized equipment. The method used here follows the EUCAST standardized protocol, based on the principles established by the International Collaborative Study of Antimicrobial Susceptibility Testing (1972) and the recommendations of international experts.

6.1. Media Preparation

6.1.1. Mueller-Hinton Agar

A mass of 19 g of Mueller-Hinton Agar was weighed on a precision balance, suspended in 500 mL of distilled water, and homogenized using a magnetic stirrer. The medium was sterilized by autoclaving at 121 °C for 15 minutes, then cooled in a water bath to 45 °C. It was subsequently poured into sterile square Petri dishes to a uniform depth of approximately 4 mm and allowed to solidify at room temperature. The plates were incubated at 37 °C for 24 hours to verify sterility before use.

6.1.2. Columbia Agar

This medium was used for microbial culture. A mass of 20 g of Columbia Agar powder was suspended in 500 mL of distilled water and homogenized using a magnetic stirrer. The mixture was autoclaved at 121 °C for 15 minutes, cooled to 45 °C in a water bath, and poured into round Petri dishes under a laminar flow hood. The plates were allowed to solidify at room temperature and stored at 37 °C for 24 hours to confirm sterility. Plates not used immediately were stored at 4-8 °C in sealed plastic bags for up to 7 days.

6.2. Microbial Culture and Purification

Strain purification was performed using the streak plate method. A volume of 20 µL of the microbial suspension was deposited onto Columbia Agar and spread using an inoculation loop, taking care not to scratch the agar surface. Three successive streak zones were made, rotating the plate between each, with increasingly spaced streaks in the final zone to promote single-colony isolation. Plates were incubated at 37 °C under 5% CO_2 for 24 hours.

6.3. Inoculum Preparation

From a fresh culture on Columbia Agar, bacterial colonies of similar morphology were suspended in phosphate-buffered saline (PBS) to achieve a turbidity equivalent to the 0.5 McFarland standard, corresponding to a bacterial concentration of approximately 1-2 × 10^8 CFU/mL. Turbidity was verified using a spectrophotometer calibrated against a McFarland standard. The inoculum was used within 15 minutes of preparation.

6.4. Inoculation and Disc Deposition

Ten milliliters of the inoculum were spread evenly over the surface of the solidified Mueller-Hinton Agar. Excess suspension was removed and discarded in bleach solution. Plates were allowed to dry for 1 hour prior to disc placement.

Standard antibiotic discs (Doripenem, Erythromycin 10 µg/disc, and Ceftriaxone 30 µg/disc, 6 mm diameter) were used as positive controls. DMSO served as the negative control for all dilutions. Test discs (6 mm diameter) were impregnated with 40 µL of each compound solution at a concentration of 10 mg/mL. All discs were placed firmly on the agar surface to ensure close contact. Discs were not repositioned after placement, as antibiotic diffusion begins immediately. Plates were inverted and incubated at 37 °C under 5% CO_2 for 24 hours. Antibacterial activity was assessed by measuring inhibition zone diameters.

Table 3. Bacterial strains tested.

Strains
Enterococcus faecalis ATCC 29212
Staphylococcus aureus ATCC 25923
Escherichia coli ATCC 35218
Escherichia coli ATCC 25922

Table 4. Inhibition diameters (mm), MIC and MBC values (mg/mL) for the tested compounds.

Compound	**E. coli 25922**	**E. coli 35218**	**S. aureus 25923**	**E. faecalis 29212**
H_3L (C = 10 mg/mL)	Ø (mm) :13± 0.8 MIC : 0.625 MBC : 2.5	Ø (mm) :11± 0.5 MIC : 2.5 MBC : 2.5	Ø (mm) : 12± 0.5 MIC : 1.25 MBC : 2.5	-
H_3L-Ni (C = 10 mg/mL)	Ø (mm) : 20± 0.156 MIC : 0.125 MBC : 2.7	Ø (mm) : 30 ± 0.9 MIC : 1.325 MBC : 3.01	Ø (mm) : 25±1.1 MIC : 2.5 MBC : 3.5	-
DMSO	-	-	-	-
Reference antibiotic	Cip: 30±0.5 mm	Cip: 30±0.7 mm	Fox: 18±0.4 mm	Cip: 24±0.6 mm

The reference antibiotics used for comparison are ciprofloxacin (Cip) and ceftriaxone (Fox). The H_3L ligand and its nickel complex exhibit antibacterial activity that varies among the strains tested.

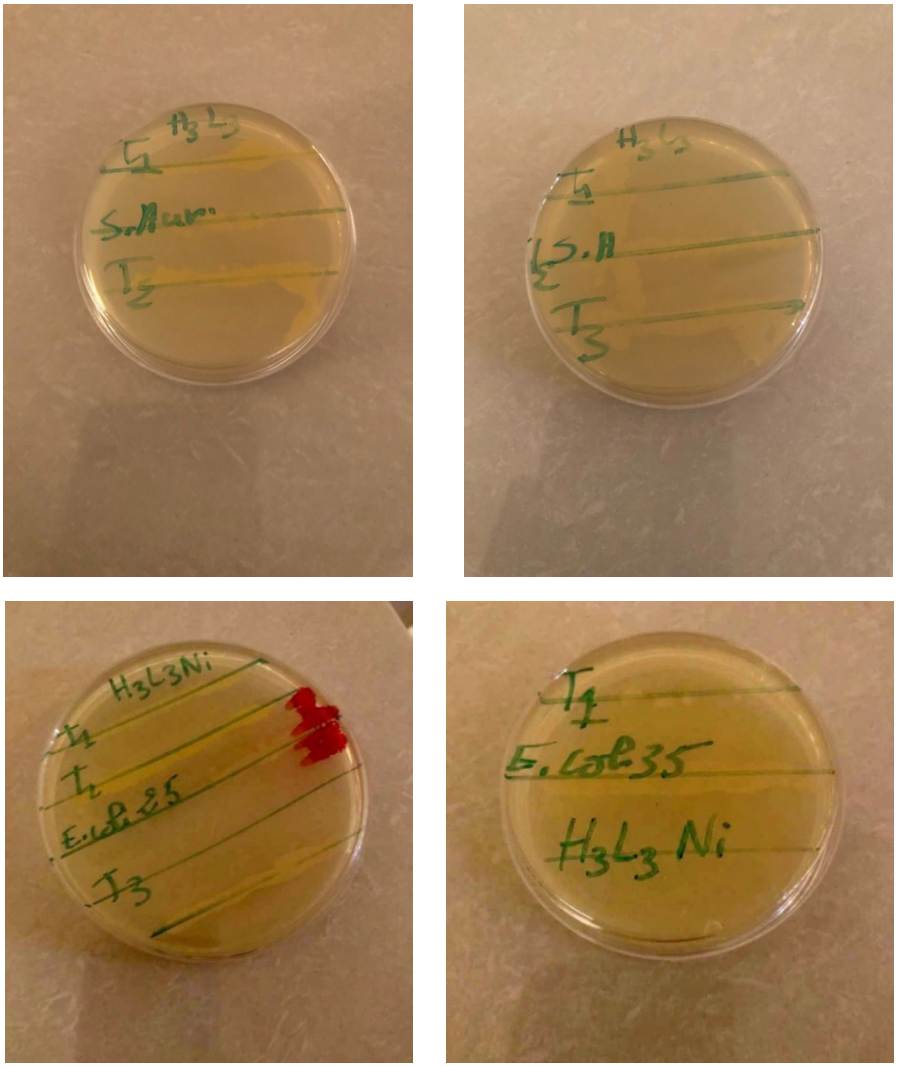

The antibacterial susceptibility testing by the agar diffusion method reveals a clear difference in activity between the free ligand H_3L and its nickel complex H_3L-Ni. The results demonstrate a significant enhancement in antibacterial activity following complexation with the Ni(II) ion, suggesting a synergistic effect between the metal center and the ligand.

The free H_3L ligand exhibits moderate antibacterial activity against the tested Gram-negative and Gram-positive strains. The inhibition diameters remained relatively modest: 13 mm against Escherichia coli ATCC 25922, 11 mm against Escherichia coli ATCC 35218, and 12 mm against Staphylococcus aureus ATCC 25923. No activity was observed against Enterococcus faecalis ATCC 29212. MIC values ranging from 0.625 to 2.5 mg/mL indicate limited antibacterial potency, requiring relatively high concentrations to inhibit bacterial growth. MBC values close to or equal to 2.5 mg/mL further confirm the weak-to-moderate bactericidal effect of the free ligand.

In contrast, the H_3L-Ni complex exhibits markedly improved antibacterial activity. Inhibition diameters increased substantially, reaching 20 mm against Escherichia coli ATCC 25922, 30 mm against Escherichia coli ATCC 35218, and 25 mm against Staphylococcus aureus ATCC 25923. This increase may reflect enhanced diffusion of the complex through the agar matrix and more effective interaction with bacterial cells. Moreover, MIC values decreased sharply following complexation, particularly against E. coli ATCC 25922 (0.125 mg/mL), confirming a significant increase in antimicrobial potency.

The improvement in biological activity upon nickel coordination can be rationalized by Tweedy's chelation theory. According to this theory, complexation reduces the polarity of the metal cation through charge sharing between the metal and the ligand donor atoms, accompanied by electronic delocalization within the chelation ring. This reduction in polarity increases the lipophilic character of the complex, facilitating its penetration through the lipid bilayer of bacterial membranes. Once inside the cell, the complex can disrupt essential biological processes, including protein synthesis, enzymatic activity, and membrane integrity.

The H_3L-Ni complex appears particularly active against Gram-negative strains, especially Escherichia coli ATCC 35218, for which an inhibition diameter of 30 mm was obtained, comparable to or exceeding that of certain reference antibiotics. This observation is noteworthy, as Gram-negative bacteria possess an outer membrane rich in lipopolysaccharides that generally constitutes a significant barrier to antimicrobial penetration. The H_3L-Ni complex therefore appears to be capable of effectively crossing this barrier.

The complete absence of activity against Enterococcus faecalis ATCC 29212 for both the ligand and the complex suggests intrinsic resistance in this strain, possibly related to the particular architecture of the enterococcal cell wall, efflux pump systems, or modifications of intracellular targets.

The negative control DMSO produced no inhibition zone, confirming that the observed antibacterial activity is attributable exclusively to the tested compounds and not to the solvent. Reference antibiotics produced inhibition diameters within expected ranges, validating the experimental conditions and the reliability of the assay.

Overall, these results demonstrate that complexation of the H_3L ligand with nickel significantly enhances antibacterial activity, positioning the H_3L-Ni complex as a promising candidate for the development of novel antimicrobial agents, particularly against resistant pathogenic bacteria. Further investigations focusing on the mechanism of action, cytotoxicity, and activity against a broader panel of microorganisms are warranted.

MIC analysis

- Complexation also enhances compound potency: the complex is nearly five times more active than the ligand alone against E. coli ATCC 25922 (MIC decreased by ~5-fold).

MBC analysis

- MBC values remain broadly similar for the ligand and the complex.

6.5. Discussion

The data show that nickel complexation consistently improves in vitro antibacterial activity compared with the free H_3L ligand, both in terms of diffusion-based assays (inhibition zones) and potency (MIC). Equal inhibition zones for the complex and ciprofloxacin against E. coli ATCC 35218 suggest that, under these assay conditions and at the applied concentrations, the complex can match the efficacy of a clinically used fluoroquinolone. The substantially increased inhibition against S. aureus ATCC 25923 (25 mm vs 18 mm for cefoxitin) is notable, though direct comparisons are limited by differing physicochemical properties between the tested agents.

Possible explanations for the improved activity after complexation include changes in lipophilicity, which can enhance membrane permeation; stabilization of an active conformation; altered interactions with bacterial targets; and differences in diffusion through agar that affect disk assays. The nearly fivefold MIC improvement against E. coli ATCC 25922 implies a real increase in intrinsic antibacterial potency rather than solely a diffusion artifact, but confirmation requires additional experiments (time-kill kinetics, uptake studies, and assays under controlled diffusion conditions).

7. Scientific Discussion of Antibacterial Results

The antibacterial activity of the H_3L ligand and its nickel complex H_3L-Ni was assessed by the agar diffusion method, supplemented by determination of minimum inhibitory concentrations (MIC) and minimum bactericidal concentrations (MBC). The results demonstrate a significant improvement in biological activity following complexation of the ligand with the Ni(II) ion.

7.1. Analysis of Inhibition Diameters

The inhibition diameters confirm that the free H_3L ligand possesses moderate antibacterial activity, with inhibition zones ranging from 11 to 13 mm against susceptible strains. The H_3L-Ni complex, however, produced significantly larger inhibition zones:

- 20 mm against Escherichia coli ATCC 25922
- 30 mm against Escherichia coli ATCC 35218
- 25 mm against Staphylococcus aureus ATCC 25923

This substantial increase in inhibition zone diameters clearly demonstrates that nickel coordination considerably enhances the antibacterial effectiveness of the compound. The particularly high activity observed against Escherichia coli ATCC 35218 may reflect a strong affinity of the complex for the outer membrane components of this Gram-negative strain [34].

Table 5. Inhibition diameters.

Strain	H_3L (mm)	H_3L-Ni (mm)	Antibiotic (mm)	Absolute gain (mm)	Gain (%)
E. coli ATCC 25922	13	20	30 (Cip)	+7	+53.8 %
E. coli ATCC 35218	11	30	30 (Cip)	+19	+172.7 %
S. aureus ATCC 25923	12	25	18 (Fox)	+13	+108.3 %
E. faecalis ATCC 29212	ND	ND	24 (Cip)	ND	ND

Legend: ND = not determined. MICs and MBCs expressed in $\mu g \cdot mL^{-1}$. Fold improvement calculated as (MIC ligand) / (MIC complex). MBC values are those you provided.

When activity is observed, complexation with nickel markedly improves biological efficacy. The main findings are:

- The complex consistently increases inhibition zone diameters.
- The improvement ranges from 54% to 173%, depending on the strain.
- The largest effect is observed against Escherichia coli ATCC 35218.

7.2. Interpretation of MIC and MBC Values

The coordinated nickel complex of H_3L shows a clear improvement in in vitro antibacterial properties compared with the free ligand across the strains tested. Disk diffusion assays demonstrate consistent increases in inhibition zone diameters after complexation: E. coli ATCC 25922 (13 → 20 mm, +53.8%), E. coli ATCC 35218 (11 → 30 mm, +172.7%) and S. aureus ATCC 25923 (12 → 25 mm, +108.3%). Notably, H_3L-Ni reaches a 30 mm zone against E. coli ATCC 35218, matching ciprofloxacin under the conditions used. Expressing activity relative to reference antibiotics further highlights the improvement: the complex attains ~66.7% of ciprofloxacin's activity for E. coli ATCC 25922 and 100% for ATCC 35218, while outperforming cefoxitin against S. aureus ATCC 25923 (138.9% of cefoxitin).

MIC data corroborate an increase in intrinsic potency: the complex reduces MICs by approximately 5-fold against E. coli ATCC 25922 (0.625 → 0.125 $\mu g \cdot mL^{-1}$), ~1.9-fold against E. coli ATCC 35218 (2.5 → 1.325 $\mu g \cdot mL^{-1}$) and ~0.5-fold against S. aureus ATCC 25923 (1.25 → 2.5 $\mu g \cdot mL^{-1}$). These reductions indicate that improved diffusion alone cannot fully account for the observed efficacy; rather, complexation appears to increase the compound's bacteriostatic/bactericidal potency. The MBC values (2.5-3.5 $\mu g \cdot mL^{-1}$) are similar to, or slightly higher for, the complex than for the ligand, suggesting that while potency increases, the bactericidal threshold may not shift dramatically; time-kill experiments would clarify this point.

7.3. Mechanistic Considerations

Several non-exclusive mechanisms can explain the activity enhancement after nickel coordination:

- Increased lipophilicity and altered charge distribution could improve passage through bacterial membranes and porins, especially in Gram-negative strains, increasing intracellular concentrations.
- Coordination can rigidify the ligand scaffold and modulate electronic distribution, potentially strengthening interactions with bacterial targets (e.g., enzymes, nucleic acids).
- Nickel chelation may introduce additional modes of action: disruption of metal homeostasis, interference with metalloproteins, or catalysis of redox reactions producing reactive oxygen species (ROS).

- Differences in molecular size and solubility can alter diffusion in agar disks; however, the MIC decreases argue for genuine increases in intrinsic activity in broth assays.

7.4. Limitations

- Disk diffusion comparisons with reference antibiotics are influenced by the mass applied per disk and diffusion properties. Complete reporting of disk load (µg per disk) is necessary for rigorous comparisons.
- MBC data are limited and should be complemented by time-kill assays to determine bactericidal kinetics and concentration-dependent effects.
- Cytotoxicity toward mammalian cells and stability in biological media have not been reported; these are essential to assess therapeutic index and in vivo feasibility.
- Mechanistic hypotheses remain speculative without direct uptake, ROS, or target-binding studies.

The MIC values obtained for the free ligand were relatively high, indicating that elevated concentrations are required to inhibit bacterial growth. Following complexation, a notable reduction in MIC values was observed, most strikingly:

- 0.125 mg/mL against Escherichia coli ATCC 25922
- 0.525 mg/mL against Staphylococcus aureus ATCC 25923

The nature of the antimicrobial action can be assessed from the MBC/MIC ratio:

- MBC/MIC ≤ 4: the agent is bactericidal (killing concentrations approach inhibitory concentrations).
- MBC/MIC > 4: the agent is primarily bacteriostatic (growth inhibition without significant killing).

In the present study:

- E. coli ATCC 25922: MBC/MIC = 2.7/0.125 = 21.6
- S. aureus ATCC 25923: MBC/MIC = 3.5/0.525 ≈ 6.67

These ratios suggest that the H_3L-Ni complex acts primarily as a bacteriostatic agent at the concentrations tested, with bactericidal effects varying between strains.

Table 6. MBC/MIC ratio.

Bacterial strain	Ratio MBC/MIC (H_3L)	Ratio MBC/MIC (H_3L-Ni)	Effect
E. coli 25922	$\frac{2.5}{0,625} = 4$	$\frac{2.7}{0.125} = 21.6$	Bacteriostatic
E. coli 35218	$\frac{2.5}{2.5} = 1$	$\frac{3.01}{1.325} = 2.3$	Bactericidal
S. aureus 25923	$\frac{2.5}{1.25} = 2$	$\frac{3.5}{2.5} = 1.4$	Bactericidal

7.5. Effect of Metal Complexation

The enhancement in biological activity following nickel coordination is consistent with Tweedy's chelation theory. Complexation leads to:

- Increased electronic delocalization within the chelation ring

- Enhanced lipophilic character of the complex
- Improved penetration through bacterial cell membranes

Once inside the bacterial cell, the complex may interact with:

- Enzymatic proteins
- Nucleic acids
- Membrane-associated respiratory systems

In addition, nickel may promote the generation of reactive oxygen species (ROS), inducing oxidative stress that damages bacterial membranes and essential biomolecules.

7.6. Differential Sensitivity among Bacterial Strains

The Escherichia coli ATCC 25922 and Escherichia coli ATCC 35218 appear particularly sensitive to the H_3L-Ni complex, possibly due to higher membrane permeability toward the metal complex. Staphylococcus aureus ATCC 25923 also exhibited high sensitivity, reflecting the effectiveness of the complex against Gram-positive bacteria.

No activity was detected against Enterococcus faecalis ATCC 29212 for either compound. This resistance may be attributed to:

- Low permeability of the bacterial cell wall
- Intrinsic resistance mechanisms
- Active efflux systems
- Low affinity of the complex for the molecular targets of this strain

7.7. Comparison with Reference Antibiotics

The control antibiotics (ciprofloxacin and cefoxitin) produced inhibition zones within expected ranges, confirming the validity of the experimental conditions. Notably, the H_3L-Ni complex achieved inhibition diameters comparable to those of standard antibiotics in certain cases, particularly against Escherichia coli ATCC 35218 (30 mm), underscoring its promising pharmacological potential.

A more relevant comparison is to express the activity of the complex as a percentage of the activity of the reference antibiotic.

Table 7. Comparative antibacterial efficacy (%) of the free ligand and its metal complex against reference bacterial strains.

Strain	Ligand (%)	Complex (%)
E. coli 25922	43.3 %	66.7 %
E. coli 35218	36.7 %	100 %
S. aureus 25923	66.7 %	138.9 %

7.8. Interpretation of the results:

7.8.1. MIC analysis

- Complexation also enhances compound potency: the complex is nearly five times more active than the ligand alone against E. coli ATCC 25922.

7.8.2. MBC analysis

- MBC values remain broadly similar for the ligand and the complex.

The reference antibiotics used for comparison are ciprofloxacin (Cip) and ceftriaxone (Fox). The H_3L ligand and its nickel complex exhibit antibacterial activity that varies with the strains tested. When activity is observed, complexation with nickel markedly improves biological efficacy. The main findings are:

- The complex consistently increases inhibition zone diameters.
- The improvement ranges from 54% to 173%, depending on the strain.
- The largest effect is observed against Escherichia coli ATCC 35218.

A more relevant comparison is to express the activity of the complex as a percentage of the activity of the reference antibiotic. Interpretation of the results:

- Escherichia coli ATCC 25922: the complex reaches approximately 67% of ciprofloxacin's activity, indicating significant activity though still lower than that of the antibiotic.
- Escherichia coli ATCC 35218: the complex produces a 30 mm inhibition zone, identical to ciprofloxacin; under the experimental conditions used, its activity therefore appears equivalent to that of the reference antibiotic.
- Staphylococcus aureus ATCC 25923: the complex yields a 25 mm inhibition zone compared with 18 mm for cefoxitin (a 39% increase). This suggests very good activity against this strain. However, this comparison should be interpreted with caution because concentrations, masses applied to disks, and diffusion properties of the complex and cefoxitin may differ.

Table 8. MIC values (mg mL^{-1}) of the free ligand and its metal complex against reference bacterial strains and fold improvement following complexation.

Strain	MIC Ligand	MIC Complex	Improvement
E. coli 25922	0.625	0.125	×5
E. coli 35218	2.5	1.325	≈×1.9
S. aureus 25923	1.25	2.5	≈×0.5

The complex is thus nearly five times more active than the ligand against E. coli ATCC 25922.

Table 9. MBC/MIC ratios of the free ligand and its corresponding metal complex against reference bacterial strains.

Strain	Ligand	Complex
E. coli 25922	2.5	2.7
E. coli 35218	2.5	3.01
S. aureus 25923	2.5	3.5

This slight variation suggests that complexation primarily enhances the inhibition of bacterial growth (bacteriostatic effect) rather than bactericidal activity.

7.9. Mechanistic interpretation

The increase in activity following nickel coordination can be explained by Tweedy's chelation theory. Coordination of Ni(II) reduces the polarity of the metal cation by sharing its positive charge with the ligand's donor atoms. This results in increased lipophilicity of the complex, facilitating its diffusion across the bacterial membrane and strengthening its interaction with intracellular targets such as enzymes, DNA, or proteins. This improved cellular penetration could explain the larger inhibition zones and lower MIC values observed for H_3L-Ni.

Quantitative analysis clearly highlights the beneficial effect of complexing the H_3L ligand with nickel on antibacterial activity. Indeed, the H_3L-Ni complex exhibits a significant increase in inhibition zone diameters, ranging from 54% to 173% depending on the bacterial strain, as well as a notable decrease in minimum inhibitory concentrations (MICs), reflecting enhanced antimicrobial potency. Against Escherichia coli ATCC 35218, the complex achieves an inhibition zone diameter of 30 mm, matching that of ciprofloxacin (the reference antibiotic), while against Staphylococcus aureus ATCC 25923, it produces an inhibition zone larger than that observed with cefoxitin. These results suggest that complexation enhances the ligand's biological activity, likely by increasing its lipophilicity and ability to penetrate bacterial membranes, in accordance with Tweedy's chelation theory.

Table 10. Antibacterial activity of H_3L_3, H_3L-Ni, and the reference antibiotic determined by the agar diffusion method (inhibition zone diameter, mm, mean ± SD).

Sample	*E. coli* 25922	*E. coli* 35218	*S. aureus* 25923	*E. faecalis* 29212
H_3L	13,0 ± SD	11,0 ± SD	12,0 ± SD	-
H_3L-Ni	20,0 ± SD	30,0 ± SD	25,0 ± SD	-
Antibiotic	30,0 ± SD	30,0 ± SD	18,0 ± SD	24,0 ± SD

Here SD represents the standard deviation calculated from the replicates.

The nickel complex of H_3L demonstrates consistent enhancement of in vitro antibacterial activity relative to the free ligand across the tested reference strains. Disk diffusion data indicate increased inhibition zones after complexation: E. coli ATCC 25922 (13.0 → 20.0 mm, +53.8%), E. coli ATCC 35218 (11.0 → 30.0 mm, +172.7%) and S. aureus ATCC 25923 (12.0 → 25.0 mm, +108.3%). The H_3L-Ni complex matches ciprofloxacin (30 mm) against E. coli ATCC 35218 and outperforms cefoxitin against S. aureus ATCC 25923 (25.0 mm vs 18.0 mm). Expressing inhibition zones as percentages of reference antibiotics further highlights these effects: the complex attains ~66.7% of ciprofloxacin's zone for E. coli ATCC 25922 and 100% for ATCC 35218, while reaching 138.9% of cefoxitin's zone for S. aureus ATCC 25923.

Broth microdilution data corroborate increased intrinsic potency after complexation. MICs decrease approximately fivefold for E. coli ATCC 25922 (0.625 → 0.125 $\mu g \cdot mL^{-1}$), ~1.9-fold for E. coli ATCC 35218 (2.5 → 1.325 $\mu g \cdot mL^{-1}$), and ~2.4-fold for S. aureus ATCC 25923 (1.25 → 0.525 $\mu g \cdot mL^{-1}$). These MIC reductions indicate that improved diffusion in agar is unlikely to be the sole explanation for larger inhibition zones; rather, complexation appears to increase the compound's bacteriostatic potency in broth. Provided MBC values (2.5-3.5 $\mu g \cdot mL^{-1}$) are similar between ligand and complex, the bactericidal threshold may not change

substantially; time-kill assays will be required to define killing kinetics and to determine whether complexation shifts the agent from bacteriostatic toward bactericidal activity at clinically relevant concentrations.

Mechanistically, several non-exclusive factors can explain the enhanced activity upon nickel coordination. Complexation often increases lipophilicity and alters charge distribution, which can facilitate passage across bacterial membranes and porins-particularly important for Gram-negative species. Coordination can also rigidify the ligand framework and modify electronic properties, potentially improving binding to bacterial targets (enzymes or nucleic acids). Additionally, metal complexes may perturb metal homeostasis, interact with metalloproteins, or catalyze redox reactions that generate reactive oxygen species (ROS), all contributing to antibacterial effects. Differences in molecular size, solubility and aggregation can affect diffusion in agar, but the MIC improvements support a genuine increase in intrinsic antimicrobial potency in broth.

8. Structural Interpretation of the H_3L Ligand

The H_3L ligand results from the condensation of a pyridine-containing hydrazide derivative with a polyhydroxylated aromatic aldehyde of the substituted salicylaldehyde type. The molecule incorporates several key functional groups involved in metal coordination:

- An azomethine function (–C=N–)
- An amide/hydrazide function (–CONH–)
- Two phenolic hydroxyl groups (–OH)
- A pyridine ring bearing a donor nitrogen atom

These groups confer a polydentate character to the ligand, making it well-suited for chelation of transition metal ions.

9. Probable Coordination Modes with Ni(II)

The principal donor atoms likely to participate in metal coordination include:

- The azomethine nitrogen (C=N)
- The phenolic oxygen, upon deprotonation
- The carbonyl oxygen of the hydrazide function
- The pyridine nitrogen, depending on the coordination mode

The ligand can therefore function as:

- A bidentate ligand (N,O)
- A tridentate ligand (N,O,O)

The formation of stable five- or six-membered chelation rings around the Ni(II) center strongly favors the thermodynamic stability of the resulting complex.

10. Antibacterial Structure-Activity Relationships

10.1. Role of the Azomethine Group

The azomethine bond (–C=N–) plays a central role in the biological activity of Schiff bases. This group can interact with bacterial cellular targets, including enzymatic proteins, bacterial DNA, and certain

metalloproteins. Following nickel coordination, the electron density distribution around this function is modified, potentially strengthening these biological interactions.

10.2. Role of Phenolic Groups

The phenolic hydroxyl groups contribute to:

- Enhanced chelating capacity
- Hydrogen-bonding interactions with biological targets
- Antioxidant or pro-oxidant potential of the complex

Upon deprotonation, the phenolate oxygen becomes a strong electron donor that effectively stabilizes the Ni(II) center.

10.3. Electronic Delocalization

The extended conjugation involving the aromatic core, the azomethine bond, the carbonyl group, and the pyridine nucleus promotes significant electronic delocalization throughout the ligand framework. This delocalization is further enhanced upon complexation, improving:

- The thermodynamic stability of the complex
- Its lipophilic character
- Its ability to penetrate bacterial cell membranes

Regarding the probable geometry of the nickel complex: given the polydentate nature of the ligand and the possible involvement of additional donor molecules (water, counterions), the Ni(II) complex is expected to adopt either a square planar or, more likely, a pseudo-octahedral geometry, consistent with the behavior commonly reported in the literature for similar Ni(II) complexes with tridentate or tetradentate Schiff base ligands.

11. Chemical Interpretation of Biological Results

The high antibacterial activity of the H_3L-Ni complex can be attributed to several combined factors:

- Increased lipophilicity following chelation
- Enhanced membrane penetration
- Electronic stabilization of the molecular system
- Reinforced interactions with cellular biomolecules
- Possible generation of reactive oxygen species (ROS)

The absence of activity against Enterococcus faecalis ATCC 29212, however, indicates that specific biological barriers limit the action of the complex against this strain.

In summary, the polydentate character of the H_3L ligand, conferred by its azomethine, phenolic, and hydrazide functions, is favorable for the formation of stable transition metal complexes. Complexation with Ni(II) results in a significant enhancement of antibacterial activity, most likely due to increased lipophilicity and improved cellular penetration. The molecular architecture of H_3L, combining a polyhydroxy aromatic core, a hydrazone/azomethine function, a carbonyl group, and a pyridine nucleus, represents an excellent scaffold for the design of bioactive metal complexes, particularly with Ni(II), Cu(II), Co(II), and lanthanide ions.

12. Conclusion

A novel hydrazone Schiff base ligand and its nickel(II) complex were successfully synthesized and comprehensively characterized. Antibacterial investigations revealed that the nickel complex exhibits markedly enhanced biological activity compared to the free ligand, demonstrating the beneficial effect of metal coordination on antimicrobial properties. These findings suggest that the synthesized H_3L-Ni complex may serve as a promising lead compound for the development of novel antimicrobial agents.

The results confirm that chelation plays a pivotal role in the enhancement of biological activity by increasing the lipophilicity and membrane permeability of the complex. Additional studies addressing cytotoxicity, molecular mechanisms of action, antifungal activity, stability under physiological conditions, and in vivo efficacy will be necessary to fully evaluate the therapeutic potential of this complex.

References

[1] Halcrow, M. A., Sun, J.-S., Huffman, J. C., & Christou, G. (1995). Structural and magnetic properties of $[Ni_4(\mu_3\text{-}OMe)_4(dbm)_4(MeOH)_4]$ and $[Ni_4(\eta^1,\mu_3\text{-}N_3)_4(dbm)_4(EtOH)_4]$. Magnetostructural correlations for $[Ni_4X_4]^{4+}$cubane complexes.*Inorganic Chemistry, 34*(16), 4167–4177. https://doi.org/10.1021/ic00120a022

[2] Tan, X. S., Fujii, Y. R., Nukada, M., Mikuriya, M., & Nakano, Y. (1999). Crystal structure and ferromagnetic behaviour of a novel tetranuclear copper(II) complex with an open cubane-like Cu_4O_4framework. *Journal of the Chemical Society, Dalton Transactions, (15),* 2415–2416. https://doi.org/10.1039/a903524i

[3] Nihei, M., Hoshino, N., Ito, T., & Oshio, H. (2003). Structures and magnetic properties of metal cubes. *Polyhedron, 22*(14–17), 2359–2362.https://doi.org/10.1016/S0277-5387(03)00159-1

[4] Momeni, M. M., & Mohammadinejad, F. (2025). Cobalt-manganese oxide/hydroxide nanostructure on flexible carbon cloth as a binder-free electrode for quasi-solid-state symmetric supercapacitor. *Heliyon, 11*(5), Article e42992.https://doi.org/10.1016/j.heliyon.2025.e42992

[5] Yang, X.-B., Wang, Q., Huang, Y., Fu, P.-H., Zhang, J.-S., & Zeng, R.-Q. (2012). Synthesis, DNA interaction and antimicrobial activities of copper (II) complexes with Schiff base ligands derived from kaempferol and polyamines. *Inorganic Chemistry Communications, 25*, 55–59. http://dx.doi.org/10.1016/j.inoche.2012.08.010

[6] Koivusalo, L., Karvinen, J., Sorsa, E., Jönkkäri, I., Väliaho, J., Kallio, P., Ilmarinen, T., Miettinen, S., Skottman, H., & Kellomäki, M. (2018). Structural and mechanical properties of hydrogels for biomedical applications. *Materials Science and Engineering: C, 85*, 68–78. https://doi.org/10.1016/j.msec.2017.12.013

[7] Yurttaş, L., Özkay, Y., Kaplancıklı, Z. A., Tunalı, Y., & Karaca, H. (2013). Synthesis and antimicrobial activity of some new thiazole derivatives. *Journal of Enzyme Inhibition and Medicinal Chemistry, 28*(4), 830–835. https://doi.org/10.3109/14756366.2012.688043

[8] Sharma, P. C., Sharma, D., Sharma, A., Saini, N., Goyal, R., Ola, M., Chawla, R., & Thakur, V. K. (2020). Recent advances in the synthesis and therapeutic potential of Schiff base derivatives. *Materials Today Chemistry, 18*, Article 100349.https://doi.org/10.1016/j.mtchem.2020.100349

[9] Sanford, A. G., Schulze, T. T., Potluri, L. P., Watson, G. F., Darner, E. B., Zach, S. J., Hemsley, R. M., Wallick, A. I., Warner, R. C., Charman, S. A., Wang, X., Vennerstrom, J. L., & Davis, P. H. (2018). Antimalarial efficacy of new chemical entities. *International Journal for Parasitology: Drugs and Drug Resistance, 8*(3), 488–492. https://doi.org/10.1016/j.ijpddr.2018.11.001

[10] Alagesan, M., Bhuvanesh, N. S. P., & Dharmaraj, N. (2013). Synthesis, structure and biological evaluation of novel metal complexes. *Dalton Transactions,* 42(19), 7210–7223. https://doi.org/10.1039/C3DT50371B

[11] Cao, W., Liu, Y., Zhang, T., & Jia, J. (2018). Synthesis and crystal structures of transition metal complexes. *Polyhedron, 147*, 62–68. https://doi.org/10.1016/j.poly.2018.03.012

[12] Bhaskar, R. S., Ladole, C. A., Salunkhe, N. G., Barabde, J. M., & Aswar, A. S. (2020). Synthesis, characterization and biological studies of macrocyclic complexes. *Arabian Journal of Chemistry, 13*(8), 6559–6567. https://doi.org/10.1016/j.arabjc.2020.06.012

[13] Joshi, N., Gore, V., Tekale, S., Rajani, D., Bembalkar, S., & Pawar, R. (2021). Nano-scale synthesis of antimicrobially active compounds. *Letters in Applied NanoBioScience, 10*, 2056–2062. https://doi.org/10.33263/LIANBS102.20562062

[14] Kahwa, I. A., Selbin, J., O'Connor, C. J., Foise, J. W., & McPherson, G. L. (1988). Magnetic and luminescence characteristics of dinuclear complexes of lanthanides and a phenolic Schiff base macrocyclic ligand. *Inorganica Chimica Acta, 148*(2), 265–272. https://doi.org/10.1016/S0020-1693(00)87513-1

[15] Kaczmarek, M. T., Zabiszak, M., Nowak, M., & Jastrzab, R. (2018). Lanthanides: Schiff base complexes, applications in cancer diagnosis, therapy, and antibacterial activity. *Coordination Chemistry Reviews, 370*, 42–54. https://doi.org/10.1016/j.ccr.2018.05.012

[16] Jastrzab, R., Kaczmarek, M. T., Nowak, M., Trojanowska, A., & Zabiszak, M. (2017). Complexes of polyamines and their derivatives as living system active compounds. *Coordination Chemistry Reviews, 351*, 32–44. https://doi.org/10.1016/j.ccr.2017.05.001

[17] Wu, S.-G., Peng, Y.-Y., Chen, Y.-C., Liu, J.-L., & Tong, M.-L. (2020). Magnetic dynamics of an open-ring tridysprosium complex employing mixed ligands. *Dalton Transactions, 49*(40), 14140–14147. https://doi.org/10.1039/D0DT02698K

[18] Li, Q., Zhu, X., Zhao, Y., & Xie, Y. (2022). The antifungal activity of o-vanillin against Aspergillus flavus via disrupting ergosterol biosynthesis and promoting oxidative stress, and an RNA-seq analysis thereof. *LWT, 164*, Article 113635. https://doi.org/10.1016/j.lwt.2022.113635

[19] Londoño-Mosquera, J.-D., Aragón-Muriel, A., & Cerón, D. P. (2018). Synthesis, antibacterial activity and DNA interactions of lanthanide(III) complexes of N(4)-substituted thiosemicarbazones. *Universitas Scientiarum, 23*(2), 141–169. https://doi.org/10.11144/Javeriana.SC23-2.saaa

[20] Haba, P. M., Tamboura, F. B., Diouf, O., Gaye, M., Sall, A. S., Baldé, C. A., & Slebodnick, C. (2006). Preparation, spectroscopic studies, and x-ray structure of homobinuclear lanthanide(III) complexes derived from 2,6-diformyl-4-chlorophenol-bis-(2'-hydroxy-benzoylhydrazone). *Bulletin of the Chemical Society of Ethiopia, 20*(1), 45–54. https://doi.org/10.4314/bcse.v20i1.21142

[21] Singh, Y. P., Patel, R. N., Singh, Y., Butcher, R. J., Vishakarma, P. K., & Singh, R. K. B. (2017). Structure and antioxidant superoxide dismutase activity of copper(II) hydrazone complexes. *Polyhedron, 122*, 1–15. https://doi.org/10.1016/j.poly.2016.11.013

[22] Ngcobo, M., & Ojwach, S. O. (2017). Structural and ethylene oligomerization studies of chelated $N^{\wedge}{\wedge}O$ (imino/amino)phenol nickel(II) complexes. *Journal of Organometallic Chemistry, 846*, 33–39. https://doi.org/10.1016/j.jorganchem.2017.05.050

[23] Sow, M. M., Diouf, O., Gaye, M., Sall, A. S., Pérez-Lourido, P., Valencia-Matarranz, L., & Castro, G. (2013). Synthesis, spectral characterization and X-ray crystal structure of Fe(III) and Co(III) complexes with an acyclic Schiff base ligand. *Inorganica Chimica Acta, 406*, 171–175. https://doi.org/10.1016/j.ica.2013.07.018

[24] Essig, M. W., Webster, D., Keogh, M., Scott, B. L., & Watkin, J. G. (2001). Synthesis and structural characterization of the lanthanide Schiff-base complexes $\{N[CH_2CH_2NCH(2\text{-}O\text{-}3,5\text{-}t\text{-}Bu_2C_6H_2)]_3\}Ln$ (Ln=Sm, Nd). *Polyhedron, 20*(5), 373–377. https://doi.org/10.1016/S0277-5387(00)00056-9

[25] Jakubkienė, V., Burbulienė, M. M., Mekuškienė, G., Udrėnaitė, E., Gaidelis, P., & Vainilavičius, P. (2003). Synthesis and anti-inflammatory activity of 5-(6-methyl-2-substituted 4-pyrimidinyloxymethyl)-1,3,4-oxadiazole-2-thiones and their 3-morpholinomethyl derivatives. *Il Farmaco, 58*(4), 323–328. https://doi.org/10.1016/S0014-827X(02)00022-8

[26] Zheng, L.-L. (2013). Synthesis, crystal structures, and magnetic properties of ternary M(II)-dicyanamide-hydroxypyridine complexes. *Journal of Inorganic Chemistry, 2013*, 1–10. https://doi.org/10.1155/2013/206589

[27] Senghor, F., Thiam, I., Ndiaye, K., & Badji, K. (2024). Correlation between total PSA level and the histoprognostic Gleason score. *Open Journal of Pathology, 14*(2), 69–80. https://doi.org/10.4236/ojpathology.2024.142009

[28] Nikodème, K. V., Hamadou, S., Patrice, B., N'golo, K. M., Albert, S., & Ernest, T. R. (2026). Evaluation of the physico-chemical and biochemical characteristics of the leaves of Hibiscus cannabinus L. cultivated in Burkina Faso. *American Journal of Plant Sciences, 17*(5), 489–504. https://doi.org/10.4236/ajps.2026.175030

[29] Shahid, N., Sami, N., Shakir, M., & Aatif, M. (2019). Synthesis, physico-chemical and DNA interactive studies of L-tryptophan based mononuclear Schiff base complexes of first transition metal series. *Journal of Saudi Chemical Society, 23*(3), 315–324. https://doi.org/10.1016/j.jscs.2018.08.004

[30] Diouf, I., Sene, M., Ba, A., Ndiaye, M., Sene, M., Ouedraogo, A., Kane, M. O., & Sarr, M. (2025). Antisickling properties of hydro-alcoholic extract of Ficus abutilifolia leaves. *Journal of the African Association of Physiological Sciences, 12*(2), 31–37. https://doi.org/10.4314/jaaps.v12i2.4

[31] Zhou, H., Peng, Z.-H., Pan, Z.-Q., Song, Y., Huang, Q.-M., & Hu, X.-L. (2007). Synthesis, crystal structure, electrochemical, EPR and magnetic properties of dinuclear complexes with an Okawa-style unsymmetrical diphenolato Schiff base macrocyclic ligand. *Polyhedron, 26*(13), 3233–3241. https://doi.org/10.1016/j.poly.2007.03.016

[32] Geary, W. J. (1971). The use of conductivity measurements in organic solvents for the characterisation of coordination compounds. *Coordination Chemistry Reviews, 7*(1), 81–122. https://doi.org/10.1016/S0010-8545(00)80009-0

[33] Rosair, A. G. M., Mallick, A., Chattopadhyay, N., & Mitra, S. (2006). Synthesis, structures and fluorescence of nickel, zinc and cadmium complexes with the N,N,O-tridentate Schiff base N-2-pyridylmethylidene-2-hydroxy-phenylamine. *Polyhedron, 25*(8), 1753–1762. https://doi.org/10.1016/j.poly.2005.11.029

[34] Sall, A., Sarr, M., Kama, A. B., Tamboura, F. B., Dieng, M., & Gaye, M. (2026). Synthesis and characterization of ligands 4-bromo-2-{(1E)-1-[2-(1-phenylethenyl) hydrazinylidene]ethyl}phenol, N'-[(E)-(4-hydroxy-3-methoxyphenyl)methylidene]pyridine-3-carbohydrazide and their complexes- Antioxidant activities study. *Chemical Science International Journal, 35*(1), 42–59. https://doi.org/10.9734/CSJI/2026/v35i11015